Indian Journal of Chemistry
Vol. 51A, Jan-Feb 2012, pp. 15-31

Potential of nanocarbons and related substances as adsorbents and chemical storage materials for H_2, CO_2 and other gases

C N R Rao*, Urmimala Maitra, K S Subrahmanyam, K Gopalakrishnan, Nitesh Kumar, Ram Kumar & A Govindaraj

International Centre for Material Sciences, Chemistry and Physics of Materials Unit,
and New Chemistry Unit Jawaharlal Nehru Centre for Advanced Scientific Research, Jakkur PO, Bangalore 560 064, India

Email: cnrrao@jncasr.ac.in

Received 15 December 2011

Solid materials which can adsorb and store hydrogen, carbon dioxide and methane are gaining importance because of the challenges faced in the energy and environment sectors. Several materials have been examined for the adsorption and storage of hydrogen. There is a notion that a material comprising light elements may be better for the adsorption and storage of hydrogen. In this context, carbon nanotubes and graphene would be expected to be suitable materials for the purpose. However, the adsorption of hydrogen on these materials reaches maximum values up to 3 to 4 wt%, that too under high pressure. Chemical storage of hydrogen in nanotubes by hydrogenation goes up to ~3wt%, but reaches a much higher value of 5 wt% or more in the case of few-layer graphenes. The sp^3 carbon-hydrogen bonds formed by the hydrogenation of graphene decompose readily on heating to ~500 ºC or on exposure to UV or laser radiation giving out all hydrogen, making few-layer graphenes attractive as possible hydrogen storage materials. Chlorine can be chemically stored in few-layer graphenes in a similar manner. Adsorption of CO_2 on activated charcoal is well known. Few-layer graphenes also adsorb CO_2 substantially, specially at low temperatures and reach values of 45 wt% at 195 K and 0.11 MPa, and 51 wt% at 298 K and 5 MPa. Graphene analogues containing B, C and N with the composition $B_xC_yN_z$ on the other hand, adsorb CO_2 up to 128 wt% at 195 K and 0.1 MPa and 64 wt% at room temperature, making them probably some of the best materials known for adsorption of CO_2. Interestingly, these BCN materials are equally good for the adsorption of methane and exhibit an adsorption of nearly 15 wt% at room temperature.

Keywords: Nanocarbons, Carbon nanotubes, Graphenes, Borocarbonitrides, Hydrogen storage, Hydrogen adsorption, Carbon dioxide adsorption, Methane adsorption, Halogen storage

The demand for energy is increasing day by day while the availability of fossil fuels is decreasing. The alarming emission of greenhouse gases, especially CO_2, is leading to undesirable changes in global climate. An attractive solution to the energy problem lies in the replacement of the fossil fuels. Chemical energy stored per mass of hydrogen (142 MJ kg^{-1}) is three times larger than that in conventional fuels (e.g. 47 MJ kg^{-1} for liquid hydrocarbons). Furthermore, hydrogen constitutes the cleanest form of energy giving off only water after burning. Hydrogen can be produced from water using a combination of photovoltaics and water electrolysis[1], although many of the routes to hydrogen are expensive. An equally serious problem is to find an affordable means of storing hydrogen.

Hydrogen can be stored in the form of compressed liquid or gas, adsorbed molecules, metal hydrides and covalently bonded molecules. The US Department of Energy (DOE) has set the energy density goal for H_2 to be used for automobiles as 6.5 wt% and 62 kg of H_2 per m^3. Since efficiency, size, weight, cost and safety issues determine the efficacy of materials for hydrogen storage, adsorption on solids seems to be one of the safe ways to store hydrogen. Activated carbon with a surface area of 500-800 m^2/g has an H_2 uptake of 1 wt% at room temperature and 10 MPa pressure.[2] Single-layer graphene is theoretically predicted to have a large surface area[3] of 2600 m^2/g, while that for few layer graphene[4] is 270 – 1550 m^2/g. Bhatia and Myers[5] calculated the optimum heat of adsorption of hydrogen on activated carbons to be 5.8 kJ/mol, while the heat of adsorption[5] needed for reversible storage of H_2 under ambient temperature and pressure is 15.1 kJ/mol. A means to achieve a high uptake of hydrogen is to vary the pore diameter leading to trapping and condensation of molecules inside the pores. Single-walled carbon nanotubes (SWNTs) with diameters generally varying in the range 0.8 – 1.2 nm are candidates for such an adsorptive storage. The curved surfaces of nanotubes provide a better binding environment compared to flat surfaces.

Another advantage of SWNTs is that they are all-surface materials, generally found in bundles with a large density of inter-nanotube pores and grooves. In SWNT bundles, four types of active sites for adsorption have been identified:[6] inner core of the nanotubes or the axial site, the inner and outer shell of each SWNT, interstitial channels between two nanotubes and the external groove sites. Cole *et al.*[7] used the anisotropic Ising model to study the nature of adsorbed gases in the interstitial channels of SWNTs. It showed that adsorbed gases undergo a phase transition to the condensed state at low temperatures inside these channels. Gases adsorbed inside the core of SWNTs undergo capillary condensation.[6] In the case of multi-walled carbon nanotubes (MWNTs), adsorption occurs by simple physisorption, the adsorption sites being the inner and outer walls. In this perspective, we discuss the adsorption of H_2 on CNTs and graphene. More importantly, we examine the nature of CNTs and hydrogenated graphenes and CNTs to explore the possible use of these materials for chemical storage of hydrogen. It is pointed out that the ready elimination of H_2 from hydrogenated graphene on heating or on exposure to suitable radiation may be usefully exploited for practical applications. We have also included discussions on graphene nanoribbons which form an important lower dimensional subset of graphenes.

Methane and carbon dioxide are major green house gases responsible for global warming. Researches to explore possibilities to minimize these gases in atmosphere are therefore absolutely necessary. Using of CO_2 in chemical reactions is one of the ways to achieve this.[8] It is however difficult to remove low concentrations of CO_2 from air using chemical reactions and a more practical way is to remove it from flue gases.[9, 10] CO_2 can be dissolved in amines,[11-21] but regeneration of the solvent by heating limits the use of this method.[22] Adsorption of CO_2 in solids would be more efficient and economical and several metal-organic frameworks (MOFs) and other solids have been investigated for this purpose.[23-32] Activated carbons are also potential CO_2 sorbents.[33,34] Though there has been considerable work on the removal of CO_2, elimination of methane from atmosphere has received somewhat less attention.

Adsorption of CH_4 in solids is generally much less effective than that for CO_2. Some MOFs have been shown to adsorb reasonable volumes of methane.[35, 36] Porous Coordination Network-14 (PCN-14) a MOF based on an anthracene derivative, 5,5′-(9,10-anthracenediyl)di-isophthalate (H4adip) and $Cu(NO_3)$, showed the highest ever CH_4 uptake of 230 *v*/*v* at 298 K and 3.5 MPa.[37] Activated charcoal and carbon fibers too show considerable CH_4 uptake.[38]

In this article, we examine the adsorption of CO_2 and CH_4 on the surfaces of nanocarbons specially graphenes prepared by different methods. What is infact remarkable is that graphene-like layered BCN exhibits very high uptake of both CH_4 and CO_2. We discuss the adsorptive properties of these and other inorganic graphene-analogues for H_2, CO_2 and CH_4 in comparison with graphene and charcoal. We also examine chemical storage of chlorine in graphene.

H_2 Adsorption

Both liquefied and pressurized hydrogen storage pose disadvantages and risks associated with sudden release. Hydrogen adsorbed on solids or stored as metal hydrides are safe methods to store hydrogen. Zeolites and metal-organic frameworks (MOFs) with tunable pores have been extensively studied for hydrogen storage applications, but have failed to reach the DOE set standards.[39-42] Metal hydrides ($LiBH_4$, $NaBH_4$, $NaAlH_4$, etc.) can reach hydrogen storage capacities as high as 18 wt%. However, high decomposition temperatures of these molecules restrict their use in reversible hydrogen storage applications.[43] Carbon-based materials such as graphene, carbon nanotubes (CNTs), especially SWNTs with high surface area and low mass density show useful adsorption properties.

H_2 adsorption on carbon nanotubes

An early report by Dillon *et al.*[44] claimed H_2 adsorption capacities of 0.01 wt% on unpurified soot containing 0.1-0.2 wt% SWNTs. Assuming only SWNTs adsorb H_2, the data was extrapolated to 5 wt% uptake of H_2 at 273 K and 300 torr. It was therefore considered that hydrogen could be condensed to high density inside SWNTs under milder conditions than that in activated carbons[44]. Liu *et al.*[45] reported H_2 storage capacity of 4.2 wt% at room temperature and 10 MPa pressure in pretreated SWNTs and showed almost complete desorption under ambient conditions. While Ye *et al.*[46] obtained a maximum of 8.25 wt% of H_2 uptake at 80 K and 120 bar in highly pure cut-SWNT ropes, Chen *et al.*[47] observed as high as 13 wt% uptake in aligned pretreated CNT_S without catalyst tips.

These results raised much hope which however did not last long. Most of the studies had been carried out on samples which were not well characterized or had high content of amorphous carbons and other metal impurities. Actual adsorption on SWNT samples turned out to be much less. Smith *et al.*[48] carried out activation of SWNTs by mild oxidation in CO_2, followed by heat treatment in inert atmosphere which increased the H_2 adsorption capacity from 0.3 wt% to 1.2 wt%. A systematic study on well characterized CNTs differing in their morphology depending on method of preparation was carried out by Gundaih *et al.*[49] MWNTs synthesized by pyrolysis of acetylene showed a low H_2 uptake while well graphitized MWNT samples prepared by arc discharge method showed adsorption of 2.6 wt% (Fig. 1(a)), which is higher than carbon fibers. Densely packed aligned MWNTs prepared by pyrolysis of ferrocene and acetylene show adsorption as high as 3.5 wt%.

On treating this sample with acid to remove catalyst nanoparticles, thereby opening up the tip, increases the H_2 uptake to 3.7 wt%. A similar observation was made in the case of SWNTs where adsorption increased from 0.2 wt% to 1.2 wt% on acid treatment. To ensure the validity of the results, independent adsorption experiments were carried out at different pressures (see Fig. 1(a) for results). At first, adsorption was monitored at high pressure followed by desorption at 300 ºC and low vacuum and then re-adsorption. A plot of wt% of H_2 adsorbed at different pressures was thus obtained (Fig. 1(b)) that showed the expected trend of decrease in storage with any decrease in pressure. To rule out the possibility of getting erroneous H_2 adsorption due to small sample weights as pointed out by Tibbetts *et al.*[50] adsorptions studies were performed using two different weights of the same MWNT sample. The shape of the adsorption curve remained the same as did the storage capacity (inset in Fig. 1(b)).

Storage of H_2 in CNTs can also be achieved electrochemically. Electrochemical storage of H_2 was shown to be comparable to gas adsorption by Gundaih *et al.*[49] with maximum storage of 3.75 wt% and charging capacity of 1050 $mAhg^{-1}$ obtained in aligned MWNTs (Fig. 2). Electrochemical charging capacity, and thus the H_2 storing capacity initially increased with cycles and ultimately reached saturation. While most of the samples studied by Gundaih *et al.*[49] required 50 cycles to reach saturation, well graphitized MWNTs required only 20 cycles to reach maximum saturation. Reversible electrochemical charging capacity of up to 800 mA hg^{-1} corresponding to 2.9 wt% of hydrogen have been reported for SWNTs.[51] The electrochemical charge discharge mechanism in the case of SWNTs was found to be somewhere between carbon nanotubes (diffusion) and that of metal hydride electrodes (reduction/oxidation).[52]

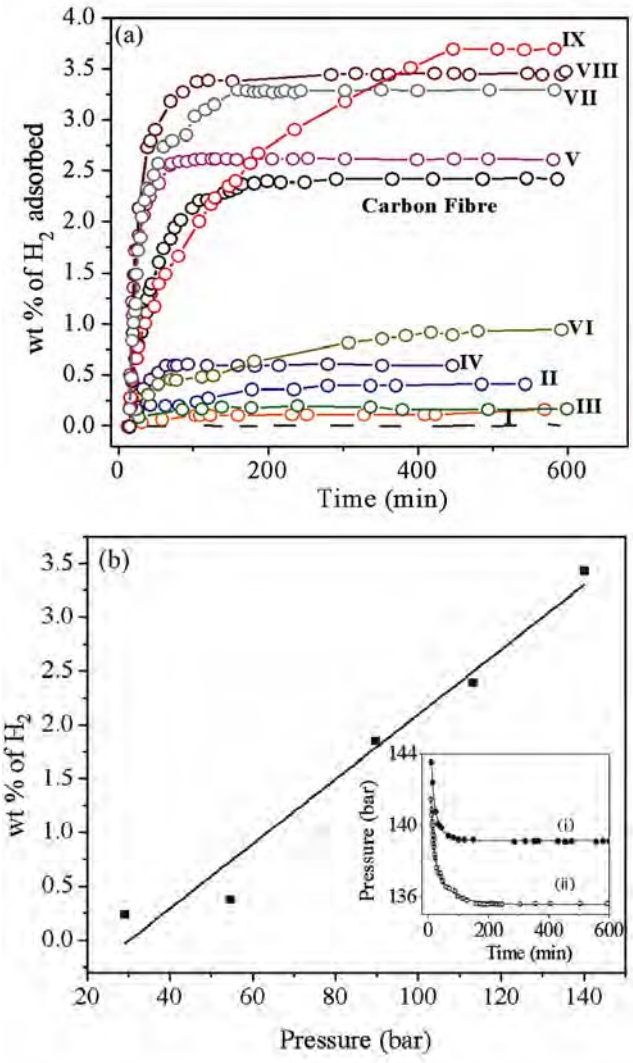

Fig. 1 — (a) Wt% of hydrogen as a function of time for carbon fiber, SWNTs synthesized by arc-discharge method, I; I treated with conc. HNO_3, II; MWNTs synthesized by pyrolysis of acetylene (as-synthesized), III; II treated with conc. HNO_3, IV; MWNTs synthesized by arc-discharge method, V; aligned MWNT bundles synthesized by the pyrolysis of ferrocene, VI; VI treated with acid, VII; aligned MWNT bundles synthesized by the pyrolysis of ferrocene and acetylene, VIII; and VIII treated with acid, IX. The broken curve represents the blank data obtained in the absence of a carbon sample. (b) Hydrogen storage in aligned MWNTs (acid-treated) sample IX at different pressures. Inset: Plots of pressure versus time for the MWNT bundles, VII, obtained with (i) 138.5 mg, and (ii) 200 mg of the sample. [Reproduced from Ref. 49 with permission from the Royal Society of Chemistry, London, UK].

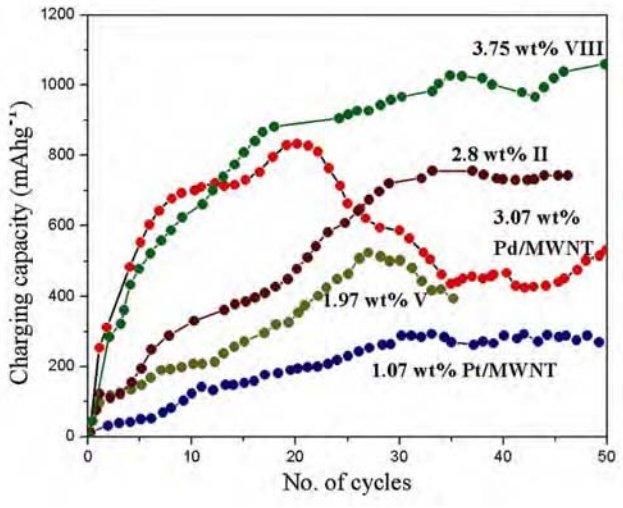

Fig. 2 — Plot of the charging capacity against the number of cycles for different carbon nanostructures. Also shown are the corresponding weight percentages of H_2 stored. [Reproduced from Ref. 49 with permission from the Royal Society of Chemistry, London, UK].

H_2 storage capacity of up to 14 wt% at ambient temperature and pressure has been reported in Li and K intercalated MWNTs.[53] The alkali metal centers seem to act as catalytically active centers for dissociative H_2 adsorption followed by spillover of dissociated H atoms to the carbon and finally getting bonded to carbon atoms. The adsorbed H_2 desorbed completely on heating to 873 K. Later experiments however indicated that the high hydrogen uptake reported were from water impurities present in the system.[54, 55] More recently, H_2 adsorption via Kubas interaction followed by dissociation of H_2 on metal particles have been reported by Reyhani *et al.*[56] in metal nanoparticle decorated with MWNTs. Pd nanoparticles turn out to be the most effective with H_2 storage capacity of 7 wt% and highest desorption onset temperature of 62 ºC. Dissociative adsorption of a H_2 on Pt and Pd decorated SWNTs has been studied by Dag *et al.*[57], suggesting a similar mechanism. SWNTs with larger diameters are shown to be better candidate for dissociative adsorption than those with smaller diameter.[57] Pd-loaded DWNTs too were shown to adsorb greater H_2 (2 wt%) than pristine DWNTs (1.7 wt%).[58] The hydrogen storage capacity of DWNTs could be significantly enhanced (3.7 wt%) by creation of defect sites by chemical activation.[58] DWNTs have been shown to adsorb much more H_2 than SWNTs despite its 40% smaller specific surface area.[59] DWNT bundles pack loosely into hexagonal bundles with interstitial pores that adsorb H_2 and were predicted to adsorb two times higher H_2 as compared to closely packed SWNT bundles. Defects induced by bombarding with C atoms or C_2 dimer at 20 eV were shown to substantially increase the molecular adsorption of H_2.[60] Average adsorption energy of H_2 molecule on defected (10,10) SWNTs created by such bombarding increased to 150 meV from 104 meV for perfect (10,10) SWNT. Even the desorption temperature enhanced from 200 K in perfect SWNT to 300 K in defected one.

H_2 uptake by BN nanotubes

BN forms nanotubes just like nanotubes since it also comprises six membered rings. As early as 2002, Ma *et al.*[61] carried out hydrogen adsorption studies on multi-walled and bamboo-like boron nitride nanotubes (BNNTs) and reported a hydrogen uptake capacity of 1.8 wt% and 2.6 wt% respectively at 10 MPa and room temperature. Tang *et al.*[62] obtained H_2 uptake as high as 4.2 wt% in so-called collapsed BNNTs. These nanotubes possessed high surface area due to numerous broken tubular shell surfaces. Thermogravimetric analysis of these nanotubes after H_2 uptake under 10 MPa for 4 h showed two weight losses at 80 and 300 ºC when 5% and 95% respectively of the adsorbed hydrogen were released. The observation indicates that not only physisorption but chemisorption occurs as well. Defects such as vacancies and dangling bonds thus energetically benefit from the saturation with hydrogen molecules or atoms allowing for such high uptake. It has been pointed out that the high uptake of the collapsed BNNTs could be due to presence of Pt which was used during fabrication of these collapsed structures. Terao *et al.*[63] obtained surface-modified, collapsed BNNTs as well as balloon-like and wool-like nanostructures of boron nitride using sulfur-containing gases during vapor–liquid–solid type synthesis. These structures showed hydrogen uptake of 1.2 wt% at 77K and 3MPa. Further proof of defect-enhanced hydrogen uptake was provided by Reddy *et al.*[64] who carried out morphology dependent hydrogen uptake studies on BNNTs and other BN nanostructures. Maximum storage capacity was shown by bamboo-type BNNTs (3 wt%) which also had the highest BET surface area. The high storage capacity of bamboo-type BNNTs was assigned to the presence of a large number of defect sites and many open-edged layers on the external surface. Straight-walled BNNTs showed a higher uptake (2.7 wt%) than flower-type BN nanostructures (2.5 wt%). This

was attributed to the easy uptake of hydrogen in the hollow tube cores of BNNTs.

Wu *et al*.[65] studied chemisorption of H atoms on zigzag (8, 0) BNNTs using DFT calculations and showed that the H adsorbed structure with 50% coverage has the highest value of adsorption energy per H_2, corresponding to 4 wt% hydrogen storage. They also showed that the H atoms prefer to bind to the top sites of adjacent B and N atoms to form an armchair type chain along the tube axis. Furthermore, the adsorption energy decreases with the increase of the radial deformation.[66] When deformation was small, hydrogen adsorption was preferred on B atoms while at large deformations, adsorption was on N atoms.

In a later work by the same group[67], dissociation of hydrogen molecule on a defect-free BN layer was found to be endothermic with a barrier greater than 2.0 eV. The dissociation barrier decreased with the decrease in tube diameter though still remaining endothermic. Layered BN and BNNTs are therefore not suitable for reversible storage of H_2. On introduction of defects like anti-sites, carbon substitution, Stone-Wales defect and vacancies, the dissociation barrier decreases and the process of dissociation becomes exothermic ensuing reversibility of adsorption.[67] Jhi[68] carried out psuedopotential density functional calculations on activated BNNTs and found that the most active pore with respect to hydrogen binding is the one passivated by oxygen, having a binding energy of about 22 kJ/mol. This is significantly larger than that of carbon nanotubes (6 kJ/mol). It is a great possibility that introduction of significant number of oxidized pores in BNNTs can therefore allow hydrogen storage at temperatures close to room temperature. Taking the ionic character of the heteropolar BNNTs bonds into account, Mpourmpakis and Froudakis[69] showed that the binding energy of hydrogen is higher in the case of BNNTs as compared to CNTs. Baierle *et al.*[70] carried out *ab initio* DFT calculations of H_2 adsorption on carbon-doped BNNTs and found a substantially higher binding energy compared to un-doped BNNT. Shevlin and Guo[71] studied the effect of 11 different types of defects (vacancies, dopants and bond rotations) on hydrogen adsorption properties of BNNTs and BN sheets. Pretreatment of BNNTs to create N-vacancies or substitution of N by dopants, especially Si appears to favour hydrogen release at relatively low temperatures (200–400 °C). In the case of BN sheets, vacancies and defects lower the dissociation energies. Curvature of nanotubes plays a role with the stress reducing the energy penalty for atoms surrounding the vacancy and the atoms surrounding the vacancy adsorbing more hydrogen and catalyzing spillover hydrogen storage.

H_2 adsorption on graphene

Patchkovskii *et al.*[72] carried out computations considering the contribution of quantum effects to the free energy and the equilibrium constant and suggested that H_2 adsorption capacities in graphene can approach values set by DOE. H_2 adsorption studies on few layer graphene samples prepared by the exfoliation of graphitic oxide (EG) and transformation from nanodiamond (DG) by Ghosh *et al.*[73] revealed a good H_2 uptake value of 1.7 wt% at atmospheric pressure and 77 K. Adsorption of H_2 was found to be directly proportional to the surface area of the samples (Fig. 3(a)). When extrapolated to single-layer graphene, the value of hydrogen uptake by EG works out to be just above 3 wt%. Adsorption of 3 wt% was achieved at 298 K and 100 atm (Fig. 3(b)). To understand the nature of adsorption of H_2 molecule on graphene, calculations have been performed within the generalized gradient approximation (GGA).[73] On the basis of relaxed geometries, two parallel and one perpendicular orientation of H_2 molecule on graphene surface was considered. For perpendicular orientation of H_2 molecule each ring in the graphene plane could stabilize one hydrogen molecule with binding energy of -3.069 kcal/mol per hydrogen molecule, leading to 7.69 wt% of hydrogen uptake for single layer graphene. With parallel orientation too, similar weight percent of hydrogen uptake was obtained with binding energy of -2.767 kcal/mol. On considering a mixture of all three different orientations, the system became stabilized at configurations with large distances between the adsorbed molecules (Inset in Fig. 3(b)). This happens at the cost of diminished H_2 uptake compared to the theoretically predicted maximum uptake of 7.69 wt%. In the case of three and four layer graphenes the uptake was predicted to be 2.7 and 2.0 wt% respectively with a desorption temperature of 203 K at 1 bar pressure.

Srinivas *et al.*[74] synthesized graphene-like nanosheets by the reduction of colloidal suspension of exfoliated graphite oxide. These sheets had surface area of 640 m^2/g and showed H_2 adsorption capacities of 1.2 wt% and 0.1 wt% at 77 K and 298 K

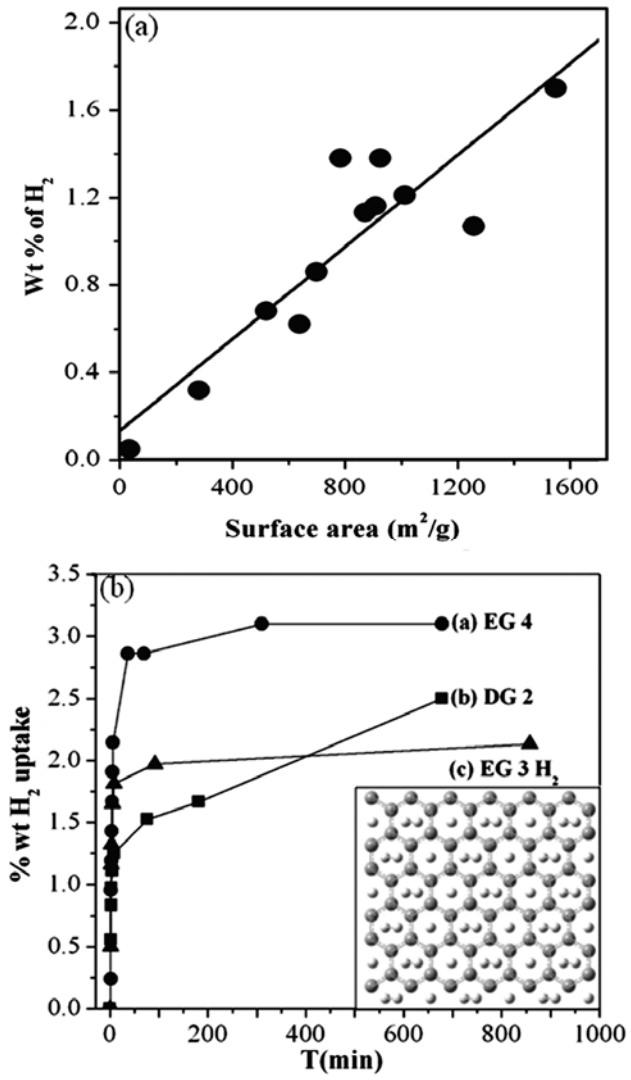

Fig. 3 — (a) Linear relationship between the BET surface area and the weight percentage of hydrogen uptake at 1 atm of pressure and 77 K. for various graphene samples and (b) High-pressure hydrogen adsorption showing the variation of the weight percentage of hydrogen uptake at 100 atm and 298 K with time for some graphene samples. Inset shows the graphene supercell with a maximum number of molecules of adsorbed hydrogen in different orientations. [Reproduced from Ref. 73 with permission from the American Chemical Society, Washington DC, USA].

respectively at atmospheric pressure. Jin *et al.*[75] reported a considerable increase in H_2 uptake in few-layer graphene by introducing cross-linkers in between graphene sheets. Hydrogen adsorption capacity could thus be tuned by varying the interlayer spacing and also the organic spacer. *Ab initio* calculations on H_2 storage capacity of alkali metal intercalated carbon nanoscrolls predicted an adsorption capacity of 3 wt%.[76]

Chemical Storage of H_2

Since adsorption of H_2 does not result in sufficient uptake, chemical storage in CNTs and graphene has been attempted. The results are summarized in the following sections.

Chemical storage of H_2 in carbon nanotubes

The strength of chemisorption of hydrogen on SWNTs is ~ 2.5 eV per H atom while that of physisorption is 0.11eV per H_2 molecule.[77] Density functional theory (DFT) calculations suggest 7.5 wt% H_2 storage in graphene through the formation of C-H bonds[77] which is close to the theoretical uptake of hydrogen by hydrogenation. Chemical hydrogenation of CNTs was first carried out by Pekker *et al.*[78] in liquid ammonia in the presence of Li metal. They obtained 0.72 wt% H_2 desorption corresponding to C:H ratio of 10.8:1. Hydrogenation was attained using atomic hydrogen beam by Nikitin *et al.*[79] XPS measurements revealed 65 at. % hydrogenation of carbon atoms, which corresponds to 5.1 wt% of H_2. The C-H bonds thus formed were stable at ambient temperature and pressure and broke completely above 600 ºC. Molecular H_2 also led to hydrogenation in CNTs at elevated temperature and pressure.[80] At 400-450 ºC and 50 bar H_2 pressure, one third of carbon atoms on SWNTs formed covalent C-H bonds. On annealing at 550 ºC, some of these nanotubes unzipped to form nanoribbons.

Hydrogenation of various types of carbon nanotubes by Birch reduction has been investigated in our laboratory. Nanotubes studied include MWNTs prepared by pyrolysis of ferrocene and acetylene, DWNTs by CVD of CH_4 over $Mo_{0.1}Fe_{0.9}Mg_{13}O$ catalyst and SWNTs prepared by arc discharge of graphite powder with Y_2O_3+Ni catalysts. Birch reduction was carried out by stirring the nanotubes with Li in dry liquid NH_3 under refluxing conditions, followed by addition of 2-methyl-1-propanol. IR spectra of hydrogenated nanotubes (MWH, DWH and SWH) clearly showed aliphatic C-H stretching bands in the 2850–2950 cm^{-1} region, while the initial nanotubes did not show a band in this region. All the hydrogenated samples showed the presence of O-H stretching in the region 3300-3600 cm^{-1}. Raman spectra of the hydrogenated samples showed an increase in the intensity of the D band, the I_D/I_G ratio increasing from 0.83 for MWNTs to 1.63 for MWH, 0.38 for DWNT to 1.01 for DWH and 0.064 in SWNTs to 0.3 in SWH. The increase in the D band intensity compared to the G band clearly indicates an

increase in the sp^3 carbon content in the hydrogenated samples. The relative increase in sp^3 carbon content was also examined by X-ray photoelectron spectroscopies (XPS). The binding energy for sp^2 and sp^3 C atoms are ~ 284.8 and 285.7 eV respectively. The ratio of sp^3 to sp^2 C was calculated from the area under each of these peaks taking capture cross section into account. On hydrogenation, the sp^3 C content increased by 28% corresponding to 1.92 wt% of hydrogen. Elemental analysis of hydrogenated sample revealed H wt% of 2.1, 2.9 and 3.9 for MWH, DWH and SWH respectively, while the initial content of hydrogen in the nanotubes was negligible.

Thermal stability and desorption behavior of the hydrogenated carbon nanotubes has been studied by heating the samples from room temperature to 650 °C (heating rate of 5 °C/min) and analyzing the released gas by gas chromatography. The samples were stable up to 350 °C and started releasing H_2 at higher temperatures. The release of hydrogen reached maximum at 400 ºC while the entire H_2 is released by 650 ºC (see Fig. 4(a)). Both DWH and SWH show similar behavior as can be seen from Fig. 4(b). The total amount of H_2 released by MWH is 1.98% while for DWH and SWH it is 3.06 and 4.04 wt% respectively. Dehydrogenated samples obtained after heating did not contain aliphatic C-H stretching bands. The intensity of the D band decreases, thereby decreasing the I_D/I_G ratio.

Chemical storage of H_2 in graphene

Hydrogenation of graphene has been carried out with hydrogen plasma[81-84] and also from molecular H_2 by catalytic hydrogenation.[85] Elias *et al.*[81] reported reversible hydrogenation of graphene films prepared by micromechanical cleavage of graphite. Hydrogenation was obtained with cold hydrogen plasma containing hydrogen-argon mixture (10% H_2). The hydrogenated sample showed electronic behavior quite different from graphene with evidence of metallic to insulator transition. The original properties of graphene were regained on heating the hydrogenated sample at 450 ºC for 24 hrs. Catalytic hydrogenation of graphene using radio frequency catalytic chemical vapor deposition (rf-cCVD) method was adopted by Zengh *et al.*[85] Ni (8 wt%) in Al_2O_3 was used as catalyst. Hydrogenation was confirmed by the appearance of peaks at 2920 cm^{-1} and 2853 cm^{-1} in (C-H stretching modes) in IR spectra and increase in intensity of D band in Raman spectrum of hydrogenated samples. They also observed that on hydrogenation, samples turned hydrophobic while the original graphene sample was

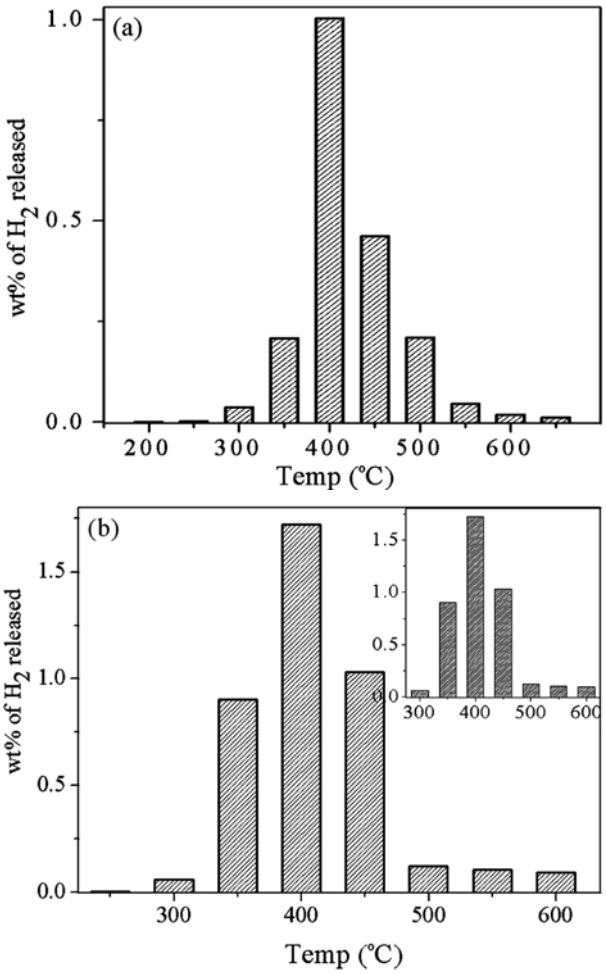

Fig. 4 — Wt% of H_2 released at different temperatures, (b) wt% of H_2 released by hydrogenated SWNTs at different temperatures. Inset shows wt% of H_2 released by hydrogenated DWNTs at different temperatures. [Unpublished results from this laboratory].

hydrophilic. We have carried out plasma hydrogenation of graphene samples prepared by arc discharge in H_2 (HG). The graphene sample was dispersed in 1,2-dichlorobenzene and coated on a glass/silicon substrate. The coated substrate was then heated in vacuum at 200 °C for 1 hour to remove any trace of solvent and then treated with pure hydrogen plasma flux of 100 W for 20 min. Elemental analysis of samples for two different plasma conditions (100 W, 20 min), one at room temperature and other at 170 °C, showed the presence of ~ 1.25 wt% and 1.78 wt% of hydrogen respectively. On plasma hydrogenation, the intensity of the D band in the Raman spectrum increased with respect to the G band while that of the 2D band decreased. Increased defect in graphene lattice caused origin of new band at 2909 cm^{-1} (D+G) as can be seen from Fig. 5.

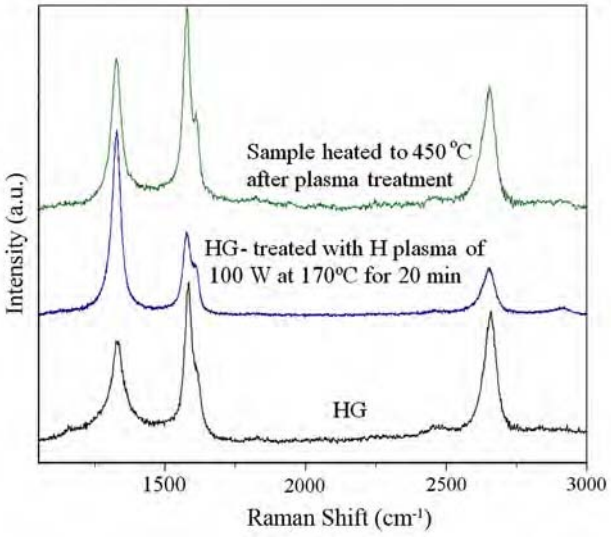

Fig. 5 — Raman spectra of the few-layer graphene, HG, before and after hydrogen plasma treatment and plasma-treated HG annealed to dehydrogenate. [Unpublished results from this laboratory].

Birch reduction of various graphene samples has been carried out by Subrahmanyam *et al.*[86] The graphene samples used for this purpose were prepared by exfoliation of graphite oxide (EG) and the arc evaporation of graphite under hydrogen (HG). The IR spectra of hydrogenated graphenes (EGH and HGH) clearly showed aliphatic C-H stretching bands in the 2850–2950 cm^{-1} region as shown in Fig. 6(a). Raman spectra showed an increase in the intensity of D band relative to G band from 0.3 to 1.7 on reduction. The UV spectrum of graphene was also affected on reduction wherein the intensity of the 260 nm band decreased progressively with the origin of a new band around 235 nm. Magnetization of the graphene samples increased on hydrogenation. Elemental analysis of reduced graphene samples showed hydrogen content to be around 5 wt%.

Thermal analysis of EGH and HGH showed that these samples were stable at room temperature for prolonged time. Heating initiates the H_2 loss, as can be seen from Fig. 6(b). Almost all the H_2 was lost by 500 °C and the sample regained its original properties. The C-H stretching band disappears and the Raman D band intensity and magnetic moment show a decrease. Dehydrogenation could also be obtained by irradiation of the hydrogenated samples with UV radiation or with a KrF excimer laser. In the case of UV irradiation, dehydrogenation occurred over a few hours (Inset in Fig. 6(a)) while with laser irradiation, dehydrogenation occurred within 2 min.

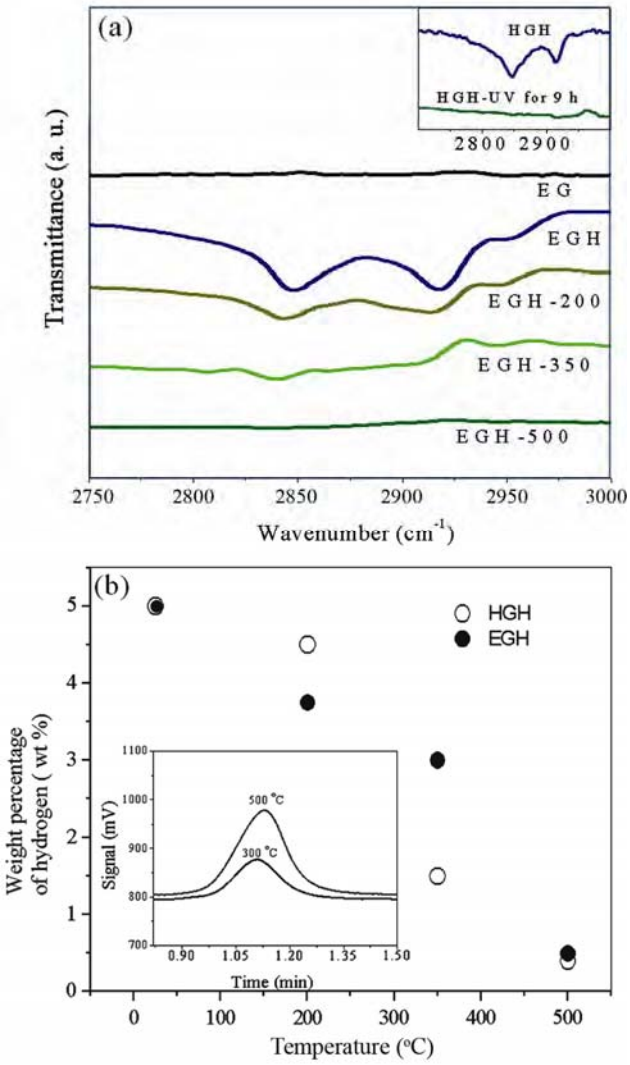

Fig.6 — (a) IR spectra of few-layer graphene (EG), Birch reduced EG (EGH) and EGH heated to different temperatures. Inset shows IR spectra of HGH and dehydrogenated HGH on UV irradiation and (b) Change in the weight percentage of hydrogen of EGH and HGH with temperature. Inset shows the evolution of hydrogen as recorded by a gas chromatograph. [Reproduced from Ref. 86 with permission from the National Academy of Sciences, Washington DC, USA].

First-principles calculations considering the interaction of hydrogen only on one side of single-layer graphene were carried out to generate conditions similar to experiments where multilayer graphene is used having very less inter-layer attraction and adsorption on the free surface only. Three different coverages, 25%, 50% and 100%, with at least two configurations in each case (one with hydrogen atoms far (>2 Å) from graphene and another with hydrogen atoms closer) were considered for the purpose. Our results revealed that 50% of hydrogen coverage,

corresponding to 4 wt% of hydrogen, had the lowest energy among the locally stable H-graphene states considered. The configurational entropy of 50% coverage was found to be greater than that for the 100% coverage, suggesting the most stable chemisorbed state of hydrogen to be half coverage with 4 wt% of H_2 uptake.

Birch reduction of graphene nanoribbons (GNR) has also been carried out. The nanoribbons were prepared by unzipping of carbon nanotubes by oxidizing agents. Elemental analysis of Birch-reduced GNRs (GNRH) showed H_2 uptake of 3 wt%. IR spectra (inset in Fig. 7) showed clear evolution of C-H stretching modes in the range 2850-2950 cm^{-1}. Thermal analysis of the sample showed H_2 loss initiating at 300 ºC and completing by 600 ºC with release of 3.05 wt% H_2 during this period. Maximum H_2 loss occurs at 400 ºC, as seen in Fig. 8. The sample starts degrading at temperatures beyond 550 ºC which might be due to the presence of some functional groups present from the initial oxidation treatment used to unzip the nanotubes.

Halogen Storage in Graphene

Chlorination of graphene (HG and EG) by irradiation with UV light in liquid chlorine medium giving rise to chlorination of 56 wt% has been examined by us.[87] The core level X-ray photoelectron spectrum of the product showed three features centered at 284.6, 285.8 and 287.6 eV corresponding to sp^2 and sp^3 hybridized carbons and C-Cl respectively as shown in Fig. 8(a). The composition of the sample as determined by the ratio of the intensity of Cl 2*p* to that of the C1*s* peak (taking into account the atomic sensitivity factors of Cl 2*p* and C 1*s*) was 30 at. % of chlorine (~ 56 wt%). The Raman spectrum of the chlorinated sample shows an increase in the intensity of the D-band relative to that of the G-band. More interestingly, chlorination is reversible. A temperature dependent stability study of the chlorinated sample showed that the sample was stable at room temperature for long periods, but slowly lost Cl_2 on progressive heating with complete loss of Cl_2 by 500 ºC. IR spectra of samples taken at various stages of heating showed progressive decrease in the intensity of the C-Cl band at 790 cm^{-1}.

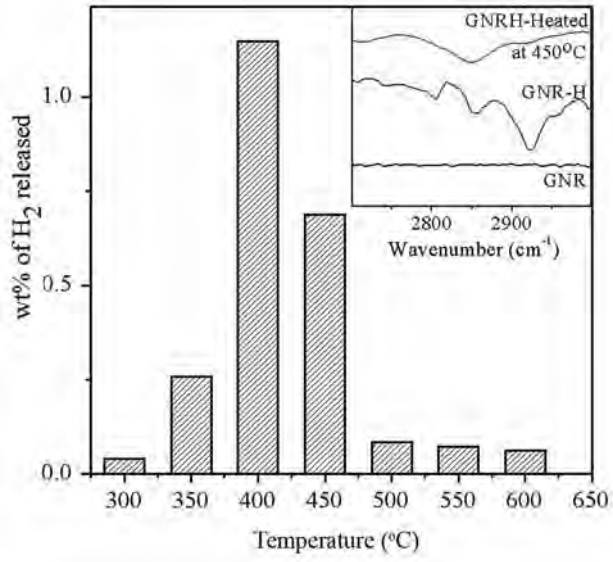

Fig.7 — (a) IR spectra of graphene nanoribbons (GNR), Birch reduced GNR (GNRH) and GNRH heated to 450 ºC to dehydrogenate and (b) wt% of H_2 released from Birch reduced GNRs at different temperatures. [Unpublished results from this laboratory].

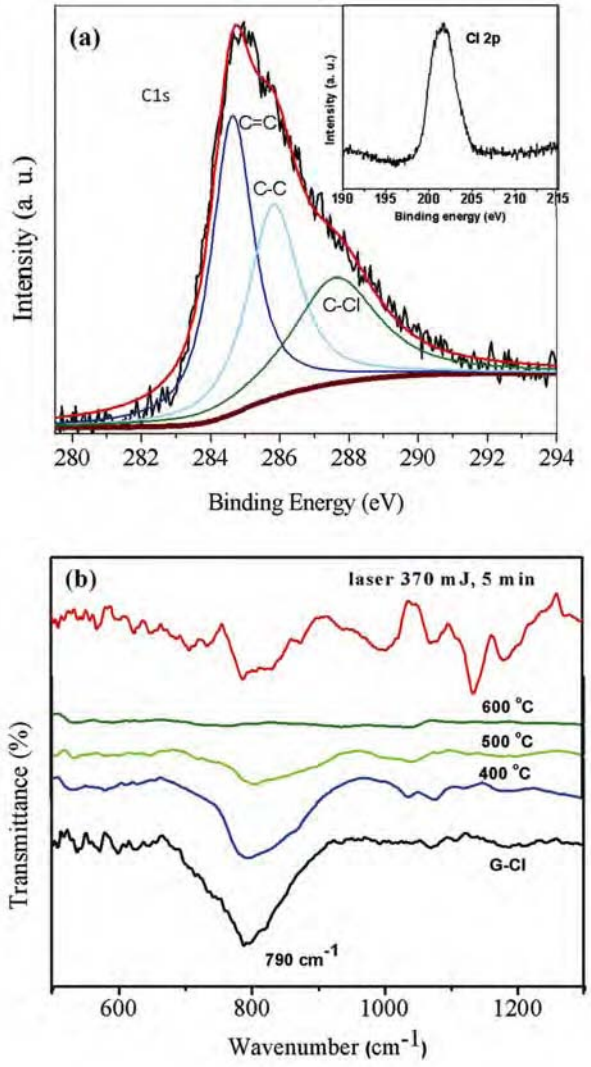

Fig. 8 — (a) C1*s* core level XP spectrum of photo-chlorinated graphene. Inset shows the Cl 2*p* signal in XPS and (b) IR spectra of the same subjected to laser radiation (370 mJ, 5 min), heated for 4 h at 400 ºC, 500 ºC and 600 ºC. [From Ref. 87].

We could also eliminate all the chlorine on irradiation with a laser (Lambda physik KrF excimer laser; λ = 248 nm, τ = 30 ns, rep. rate = 5 Hz, laser energy = 370 mJ) as shown in the inset in Fig. 8(b). Dechlorination appears to be associated with a small barrier just as the decomposition of hydrogenated graphene. The strain in the chlorinated sample appears to drive the dechlorination to form the more stable graphene. Bromination of graphene up to 25 wt% could be achieved and the bromine is fully eliminated by 500 ºC. The study demonstrates that few-layer graphene can be used to store chlorine and bromine.

Methane Adsorption

Methane adsorption on CNTs

Metal-organic frameworks, zeolites and porous membranes are known to store methane, but sp^2 carbon materials, mainly carbon nanotubes, seem to offer a greater promise to storage of methane. Theoretical work on the adsorption of methane is mainly concentrated on SWNTs, which generally exists in bundles. The potential binding sites for CH_4 in SWNTs are linear interstitial channels, outer peripheral walls, the grooves between two outer nanotubes in the bundles and the external surfaces.[88,89] Johnson and co-workers[90-92] studied the effect of defects and interstitial channels in SWNT bundles on the adsorption of gas molecules including methane and concluded that if a heterogeneous distribution (packing of SWNTs of different diameters) is considered, the packing defects can cause relatively large interstitial channels giving rise to high methane uptake. Kowalczyk *et al.*[93] considered storage of methane at 293 K and up to 8 MPa in idealized bundled of (10,10)-armchair SWNTs and carbon worm-like pores by molecular simulation techniques with VDWG of 0.4 nm. They show that these materials achieve a methane uptake of 5.4 MJ dm^{-3} (meeting the US Freedom CAR Partnership target of 2010) at low pressures while 13 MPa is required to compress methane in order to get the same volumetric energy density.

The first experimental realization of methane storage in carbon nanostructures was reported by Bekyarova *et al.*[94] who showed that single-walled nanohorns (SWNH) with an interconnected network structure could store 160 *v*/*v* methane at 3.5 MPa and 303 K. Murata *et al.*[95] reported an enhancement of adsorption of methane by dispersing lanthanide nitrate on the nanocarbons. According to them, lanthanum nitrate distorts the electron cloud of the nano carbon and affects the interaction between SWNHs and methane. Yamamoto *et al.*[96] varied bundle parameters by drying well isolated SWNTs in different organic solvents and confirmed the contribution of the negative curvature of the internal wall of the tubes and the interstitial pores in the adsorption of methane on SWNT bundles. The uptake of CH_4 is less in MWNTs as compared to SWNTs because of the absence of sites like interstitial channels, outer grooves, etc. Lee *et al.*[97] explained the adsorption of methane on MWNTs on the basis of a combined model containing both Langmuir and Sips contributions. They could achieve an uptake of ~ 3 wt% at 303.15 K and 3 MPa. By mixed acid treatment, alkali treatment and mechanical shearing, Yulong *et al.*[98] found that the uptake of methane in MWNTs can be enhanced to a value as high as 11.7 wt% at room temperature and 10.5 MPa.

Methane adsorption on graphenes

Albesa *et al.*[99] studied methane adsorption on graphite surface by using Monte Carlo simulations (MCSs) of the grand canonical ensemble (GCE) and mean-field approximation (MFA). These workers confirmed layer by layer mechanism of adsorption of CH_4. The isosteric heat of adsorption was calculated to be 13 kJ/mol. Thierfelder *et al.*[100] used DFT calculations to study the adsorption of methane on graphene and obtained an adsorption energy of 0.17 eV and a molecular distance of 3.28 Å. They identified four probable high-symmetry adsorption sites with the H-tripod oriented towards the substrate or the vacuum.

Adsorption of methane has been studied in this laboratory on four graphene samples, EG, HG, RGO and SGO, and compared with high surface area activated charcoal.[101] EG was prepared by thermal exfoliation of graphitic oxide, HG by evaporation of graphite in hydrogen, SGO by ultrasonication of graphitic oxide and RGO by reduction of SGO. The surface areas of the graphene samples and activated charcoal vary between 5 and 1250 m^2/g. Among the graphene samples, EG shows the highest surface area with a value of 640 m^2/g, and SGO the lowest value of 5 m^2/g. Activated charcoal had a surface area of 1250 m^2/g. Adsorption of methane on the graphenes and activated charcoal was measured at 273 K and 298 K. The weight uptake of methane by activated charcoal is 7 and 6 wt% at 273 K and 298 K and 5 MPa respectively. The CH_4 uptake of the graphene

samples varies between 0 and 3 wt% at 273 K and 5MPa. Typical CH_4 adsorption data of EG at 298 K and 5 MPa is shown in Fig. 9(a). Adsorption isotherm for activated charcoal has been shown in the inset for comparison. Figure 9(b) shows the methane uptake of graphene samples as well as activated charcoal against their surface areas. EG and RGO with relatively high methane uptake contain oxygen functionalities on the surface, while in the case of HG with clean surface there was little or no uptake of methane.

Methane adsorption on graphene analogues

Graphene analogues have not been well explored for gas adsorption properties. Janik *et al.*[102] studied methane and CO_2 adsorption on eight different boron nitride samples at 273 K and 800 torr prepared by taking different precursors and processing routes. Despite similar surface areas these BN samples showed a distribution in methane adsorption, indicating the presence of special binding sites.

Borocarbonitrides ($B_xC_yN_z$) have been recently explored by us for methane adsorption.[101] The BC_xN samples were prepared by mixing boric acid, high surface area activated charcoal and urea in different proportions and heating at high temperature in order to get samples with different compositions and surface areas. The surface areas of these samples vary between 1990 m^2/g (BCN-5) and 1509 m^2/g (BCN-1). Typical CH_4 uptake by high surface area BCN-5 at 298 K and 5 MPa is shown in Fig. 10(a) with that at 273 K and 5 MPa in the inset. The CH_4 uptake value varies from 7.5 to 17% CH_4 at 273 K. At 298 K, it is 5 wt% for BCN-1 and 15 wt% for BCN-5. Uptake of 15 and 17 wt% at 273 and 298 K by BCN-5 is comparable to the highest values of CH_4 uptake

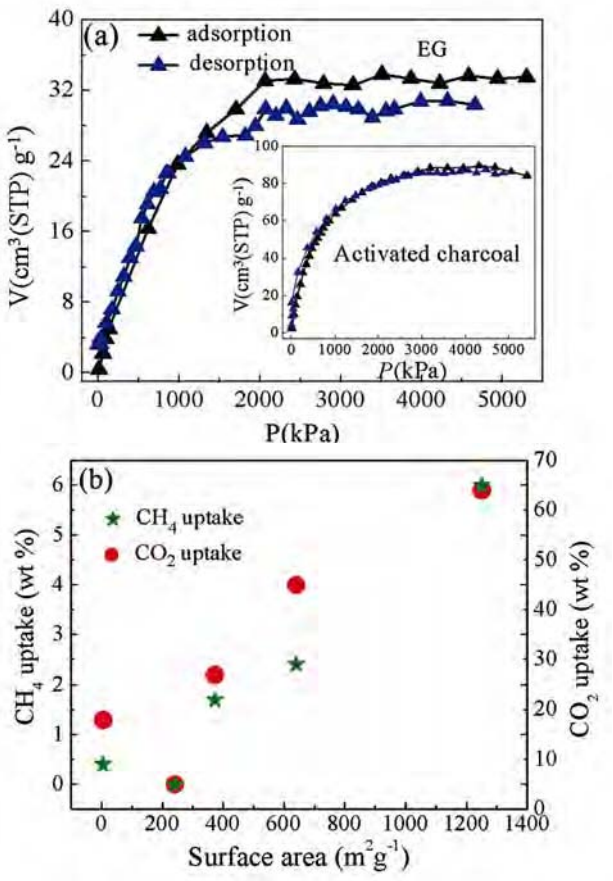

Fig. 9 — (a) Methane adsorption-desorption isotherms of few-layer graphene (EG) at 298 K and 5 MPa, while the inset shows the corresponding isotherms for activated charcoal at 298 K and 5 MPa; (b) Plot of the weight percentage of methane uptake (at 298 K and 5 MPa) and CO_2 uptake (at 195 K and 1 atm) versus the BET surface area. [Reproduced from Ref. 101 with permission from Wiley-VCH, Weinheim, Germany].

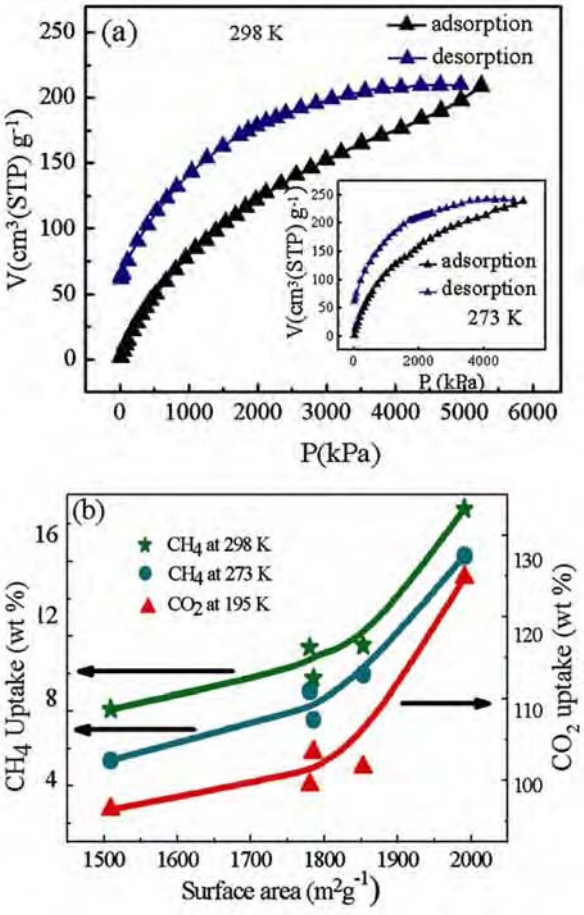

Fig. 10 — (a) Methane adsorption-desorption isotherms of BCN-5 at 298 K and 5 MPa. Inset shows the corresponding isotherms at 273 K and 5 MPa; (b) Plot of the BET surface area versus the weight percentage of methane uptake at 273 and 298 K and 5 MPa and CO_2 uptake at 195 K and 1 atm. [Reproduced from Ref. 101 with permission from Wiley-VCH, Weinheim, Germany].

reported in the literature. The uptake of CH_4 increases nearly exponentially with the surface area (Fig. 10(b)). This observation may be taken to indicate that these gases may have specific interaction with high surface area $B_xC_yN_z$ samples, possibly due to the presence of specific structure entities unique for these compositions. To support our experimental findings, we carried out first-principles calculations on the adsorption of CH_4 on BC_xN. In order to avoid errors in density functional theory-based estimation of adsorption energies due to neglect of van der Waals interaction, we employed DFT-GGA (density functional theory - generalized gradient approximation) based analysis of the adsorption of the methane on BCN atomic sheets. Based on the adsorption of methane on BCN with lowest coverage (7 wt%, one methane molecule per supercell), the following sites were found to be strongly adsorbing: (a) boron bonded with at least one carbon atom which is likely to be a weakly negative ion, (b) hexagonal ring consisting of at least two carbon atoms along with B and N, and, (c) carbon bonded with two boron atoms, which would develop a slightly negative charge to attract the molecule (Fig. 11(a)). Methane showed lower adsorption energy on BCN surface as compared to graphene at all % coverages. For example at 7% coverage adsorption energy on BCN was –2.08 kJ mol^{-1} stronger than –1.97 kJ mol^{-1} for graphene and at 13%, it was –2.72 kJ mol^{-1} for BCN as compared to –2.27 kJ mol^{-1} for graphene. Methane when adsorbed on graphene, BN and BCN was found to develop a small electric dipole moment (considering electrostatic interactions) at low coverages which turned out to be strongest on BCN. Thus at all coverages of CH_4 on BCN adsorption was somewhat stronger than that on graphene. Our results established the optimal storage of methane on BCN at 18 wt%.

CO_2 Adsorption

CO_2 adsorption on CNTs

High surface area materials such as activated charcoal are good candidates for CO_2 adsorption since they have high adsorption capacities and are much cheaper than other sequestration methods. Zhao *et al.*[103] employed DFT calculations with local density approximation to study the adsorption of a variety of gases including CO_2 on isolated SWNTs and tube bundles. CO_2 was found to be a charge donor with an average of 0.014 electron donation per molecule. Chen and Johnson[104] focused on the adsorption of CO_2 on groove sites in bundles of SWNTs. Atomistic simulations have shown that CO_2 clusters adsorbed in the groove sites at low temperatures contain an odd number of molecules and the molecules in the clusters are orientationally ordered. Such clustering and orientation were attributed to the delicate balance between van der Waals and solid-fluid forces and the fluid-fluid quadrupole and van der Waals forces. Kowalczyk *et al.*[105] have studied the pore size effect on the volumetric and gravimetric storage of CO_2 on bundles of SWNTs by grand canonical Monte Carlo simulation (GCMC) simulations and they showed that at 3.5 MPa and 298 K the optimum diameter is 4.8 nm corresponding to a gravimetric and volumetric storage of 25.3 mmol g^{-1} and 16.7 mol dm^{-3} respectively. They compared the most efficient CO_2 storage material, MOF-177[106], with SWNTs and concluded that although the MOF has a high gravimetric uptake (21.8 mmol g^{-1} compared to 13.6 mmol g^{-1} in SWNT at 1.5 MPa and 298 K), the volumetric storage of

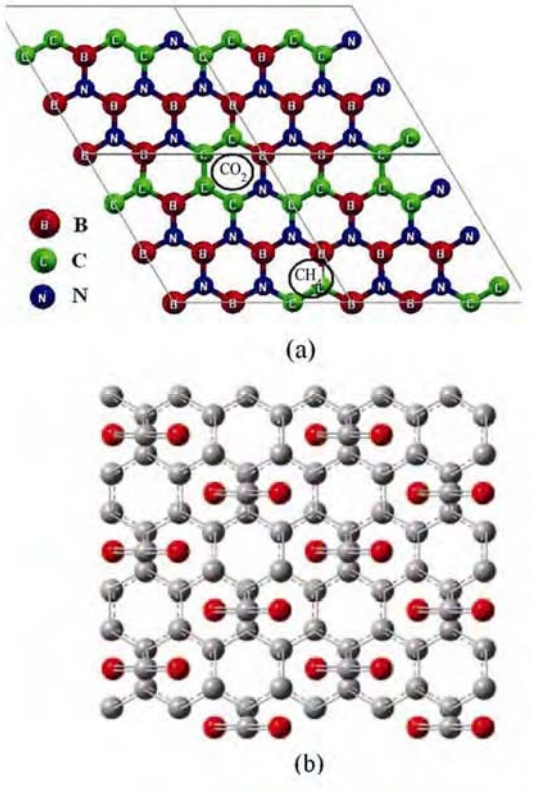

Fig. 11 — (a) Preferred sites of CH_4 and CO_2 adsorption on BCN. [Reproduced from Ref. 101 with permission from Wiley-VCH, Weinheim, Germany] and (b) Graphene supercell containing 72 carbon atoms with maximum number of CO_2 molecules on one side. [Reproduced from Ref. 73 with permission from the American Chemical Society, Washington DC, USA].

SWNTs is better (11.4 mol dm^{-3} compared to 12.26 $moldm^{-3}$ in MOF-177 at 1.5 MPa and 298 K). Mackie and Dilabio[107] carried out DFT calculations in order to study CO_2 adsorption in the interior and exterior of pristine and nitrogen doped SWNTs. They predicted a larger binding energy up to 9.1 kcal mol^{-1} for zig-zag SWNT compared to the armchair (8.3 kcal mol^{-1}) and chiral (7.0 kcal mol^{-1}) SWNTs. Doping zig-zag SWNTs with nitrogen increased the binding energy by 3 kcal mol^{-1}, while a slight reduction in binding energy was observed in armchair as well as chiral SWNTs.

An early experimental study of CO_2 adsorption on SWNTs was carried out by Cinke *et al.*[108], where they compared the adsorption properties of as received HiPCo, purified HiPCo and activated carbon in the temperature range of 273 – 473 K. As received HiPCo samples showed influence of the presence of iron and iron oxide, while the purified HiPCo gave proper type II adsorption isotherm. When compared to activated carbon, HiPCo showed double CO_2 uptake though the surface area was only 25% larger. Hu and Ruckenstein[109] studied CO_2 adsorption on Carbolex SWNTs by fitting the isotherms at 273 and 298 K using Dubinin–Astakhov equation. They obtained Astakhov exponent of less than 2 (n = 1.68, indicating the presence of heterogeneous porosities and CO_2 adsorption on both inner and outer walls. Similar surface areas were obtained from the CO_2 adsorption isotherm by this method as that obtained from BET surface area isotherms. Bienfait *et al.*[110] studied adsorption of several gases including CO_2 by adsorption isotherms, isosteric heat of adsorption and neutron diffraction measurements. These workers observed a completely different trend in the case of CO_2 which unlike other gases mainly adsorbed at the grooves. The difference was attributed to the entropic effects and less adsorption of CO_2 on graphitic surfaces. They observed isosteric heat of adsorption value of 22.5 kJ mol^{-1} on highly binding sites. Mishra and Ramaprabhu[111] studied CO_2 adsorption in the composites of MWNT and magnetite nanoparticles. At all the temperature and the pressure ranges the nanocomposite showed a large increase in the adsorption as compared to the MWNTs alone. The enhancement in the adsorption was attributed to the additional chemical interaction of magnetite nanoparticles and CO_2 in nanocomposite.

There are several reports of CO_2 adsorption on the amine-functionalized carbon nanotubes. Lu and co-workers[112-114] compared the adsorption properties of pure and 3-aminopropyl-triethoxysilane (APTS) functionalized MWNTs at a temperature range of 293 – 373 K. They showed an increase of more than 40% of CO_2 adsorption at 293 K and influent flow of 50 mg L^{-1}. They also showed that the adsorption and physiochemical properties of APTS modified MWNT remain preserved even after 100 adsorption-desorption cycles. The water vapor content also influenced the adsorption properties with a maximum adsorption of 2.4 mmol g^{-1} at 2.4% water vapour and 323 K. Dillon *et al.*[115] studied the effect of polyethyleneimine (PEI) functionalization on fluorinated SWNTs (FSWNTs). A maximum adsorption of 9.2 wt% could be achieved at 27 K and 1 atm of CO_2. Matranga *et al.*[116,117] found that thermolysis of mildly oxidized SWNTs resulted in entrapped CO_2 molecules. The molecules appear to remain trapped tentatively in the endohedral and interstitial sites up to temperatures as high as 700 K.

CO_2 adsorption on graphenes

Cabrera-Sanfelix[118] predicted that both physisorption and chemisorption of CO_2 occur on graphene based on DFT calculations of CO_2 adsorption on single-layer of graphene. Physisorption occurs on the top of the vacancy defects, with the axis of the CO_2 molecule parallel to the surface with binding energy of ~136 meV. The physisorbed molecule then gets chemisorbed forming a lactone with energy release of 1.4 eV. The global pathway is therefore energetically feasible. Mishra and Ramaprabhu[119] studied adsorption of CO_2 on magnetite decorated graphite nanoflakes prepared by acid intercalation followed by thermal exfoliation. They observed an enhancement of 90% in the uptake of CO_2 at 298 K and 50 bar pressure on decorating graphite nanoflakes with magnetite nanoparticles. The uptake of CO_2 by several few-layer graphene EG, HG, RGO and SGO have been studied in this laboratory[101] and compared with that of activated charcoal. Typical CO_2 adsorption data of EG at 195 K and 1 atm has been shown in Fig. 12(a) in comparison with that of activated charcoal (inset Fig. 12(a)). Activated charcoal showed 64 wt% uptake of CO_2 at 195 K and 1 atm while uptake of CO_2 by EG at 298 K and 50 bar was 51%. The uptake values varied between 5 and 45 wt% in the case of graphene samples at 195 K and 0.1 MPa with EG exhibiting the highest uptake. EG and RGO samples with relatively high CO_2 uptake capacity contain oxygen functionalities on the surface while HG with relatively clean surface did not show

considerable uptake. However, all the graphenes exhibit smaller uptake capacity for CO_2 compared to activated charcoal which too is known to have a large number of surface functional groups. Figure 9(b) shows the dependence of CO_2 uptake on the surface area of the graphene samples. The uptake varies nearly exponentially with surface area and follows same the trend as CH_4. Calculations on the adsorption of CO_2 on graphene have been carried out within generalized gradient approximation (GGA).[73] Three different configuration with CO_2 parallel to graphene lattice was considered to obtain an adsorption maximum of 12 CO_2 molecules adsorbed on one side of the graphene super cell with 72 carbon atoms (Fig. 11(b)) exhibiting a binding energy of –14.112 kcal/mol. This suggested maximum CO_2 uptake of 37.98 wt% for single layer graphene and 16.92 and 13.25 wt% for three and four layered samples respectively. A desorption temperature was calculated to be 657 K at 1 bar pressure using the van't Hoff equation for the estimation of the entropy of vaporization of carbon dioxide.

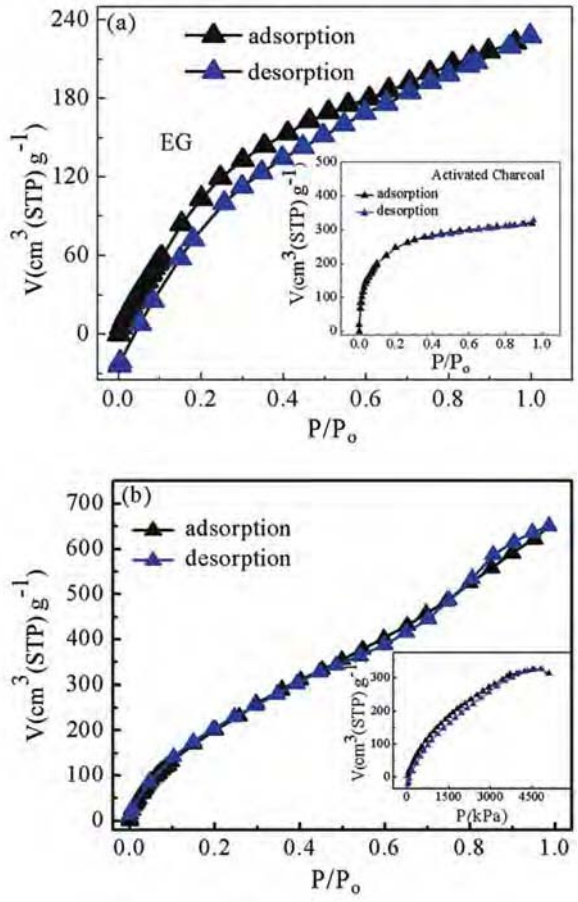

Fig. 12 — (a) CO_2 adsorption-desorption isotherms of few-layer graphene (EG) with those of activated charcoal in inset at 195 K and 1 atm and (b) CO_2 adsorption-desorption isotherms of BCN-5 at 195 K and 1 atm. Inset of (b) shows the corresponding isotherms of at 298 K and 5 MPa. [Reproduced from Ref. 101 with permission from Wiley-VCH, Weinheim, Germany].

CO_2 adsorption on bocarbonitrides

Boroncarbonitrides, $B_xC_yN_z$ with surface areas ranging between 1990 m^2/g (BCN-5) and 1509 m^2/g (BCN-1) are found to be excellent adsorbents for CO_2.[101] BCN-5 showed a CO_2 uptake of 128 wt% at 195 K and 1 atm as can be seen in Fig. 12(b). A remarkable CO_2 uptake of 64% was observed even at room temperature and 50 bar pressure (inset in Fig. 12(b)). The CO_2 uptake too varied nearly exponentially with surface area as in the case of CH_4 (Fig. 10(b)). CO_2 adsorption is known to occur strongly at the following atomic sites in BCN[120]: (a) nitrogen bonded with at least one carbon atom which is likely to be a weakly negative ion, (b) boron bonded with one nitrogen atom and one carbon atom, which would attract negatively charged oxygen of the molecule, and, (c) a hexagonal ring with 4 carbon atoms forming the hexagonal ring and a boron and a nitrogen atom (Fig. 11 (a)). Figure 13 shows the variation of adsorption energy in the case of graphene

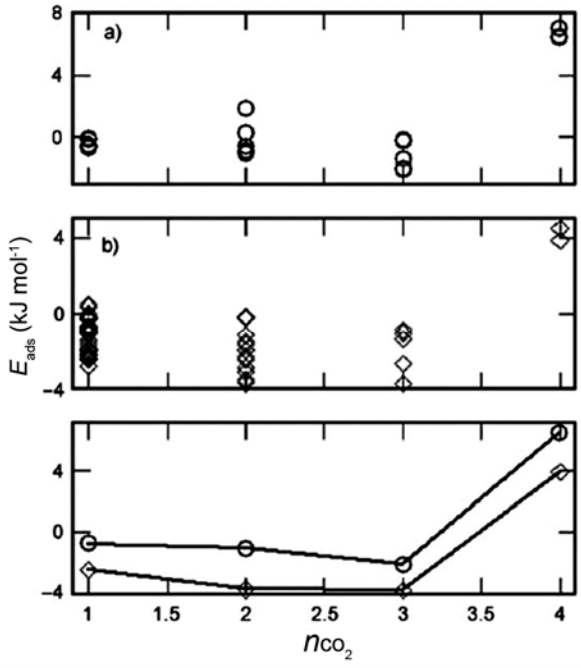

Fig. 13 — Energies of adsorption of CO_2 molecules at different coverages (n molecules per 18 atom cell) with different configurations of adsorption sites in (a) graphene, (b) BCN. (c) Comparison of energies for the strongest adsorption of CO_2 on graphene (o) and BCN (◊).[Reproduced from Ref. 120 with permission from Wiley-VCH, Weinheim, Germany].

and BCN at different CO_2 coverages for different configurations of adsorptions. For 20 wt% coverage of CO_2 on BCN, the calculations show that the adsorption of CO_2 at the centre of a certain hexagonal ring is stronger than that at the atomic sites. The rings which show strong adsorption of CO_2 have typically at least two carbon atoms and a pair of B and N atoms. Moreover, rings with corner atoms (which are weak adsorbing sites) usually have stronger adsorption at the surface. Among the various orientations of the CO_2 molecules lying flat on the ring, the one with the axis along the C-B or C-N diagonal of the ring is energetically more favourable. At 20 wt% coverage for the lowest energy configuration, the CO_2 adsorption energy is 2.79 kJ mol^{-1} compared to only 0.79 kJ mol^{-1} for graphene. At this coverage, the CO_2 molecule is about 3.71 Å above the BCN plane as compared to 3.83 Å in graphene. At a higher coverage value of 40 wt%, the interaction among nearby CO_2 molecules becomes important and the adsorption of CO_2 molecule closer to the atomic sites becomes favorable. Adsorption energy of CO_2 on BCN is 3.67 kJ mol^{-1} compared to 1 kJ mol^{-1} on graphene. At an even higher value of 60 wt% the CO_2 adsorption energy on BCN is 3.73 kJ mol^{-1} compared to 2.04 kJ mol^{-1} in graphene. Also, the orientation of CO_2 molecule is mixed, two in plane and one perpendicular to the plane. At 80 wt% coverage, the adsorption is not favourable because of the interaction between CO_2 molecules.

Conclusions

From the foregoing discussion, it becomes clear that adsorption of hydrogen on carbon nanotubes and graphene does not reach sufficiently high values to make them potential materials for possible use in automobiles or elsewhere. However, chemical storage of hydrogen in few-layer graphenes is sufficiently high (5 wt% or more) to be considered for possible use in appropriate situations. What is interesting is that the storage of hydrogen in graphene is chemical in nature where the sp^2 carbons are converted into sp^3 carbons and the sp^3 carbon-hydrogen bond dissociates giving rise to hydrogen at relatively low temperatures. That these C-H bonds are dissociated photolytically is noteworthy. In terms of chemistry it is interesting that halogens such as chlorine can also be stored in few-layer graphene through the formation of sp^3 carbon-chlorine bonds, these bonds being broken thermally or photolytically. As far as CO_2 and methane are concerned few-layer, graphenes show reasonably good adsorption but not comparable to activated charcoal. Graphene-like materials containing boron carbon nitrogen with the general composition $B_xC_yN_z$, on the other hand, exhibit high adsorption of both CO_2 and CH_4. Study of such materials containing light elements deserves further exploration.

References

1 Gratzel M, *Nature*, 414 (2001) 338.
2 de la Casa-Lillo M A, Lamari-Darkrim F, Cazorla-Amors D & Linares-Solano A, *J Phys Chem B*, 106 (2002) 10930.
3 Peigney A, Laurent C, Flahaut E, Bacsa R R & Rousset A, *Carbon*, 39 (2001) 507.
4 Rao C N R, Sood A K, Voggu R & Subrahmanyam K S, *J Phys Chem Lett*, 1 (2010) 572.
5 Bhatia S K & Myers A L, *Langmuir*, 22 (2006) 1688.
6 Calbi M M, Cole M W, Gatica S M, Bojan M J & Stan G, *Rev Mod Phys*, 73 (2001) 857.
7 Cole M W, Crespi V H, Stan G, Ebner C, Hartman J M, Moroni S & Boninsegni M, *Phys Rev Lett*, 84 (2000) 3883.
8 Yu K M K, Curcic I, Gabriel J & Tsang S C E, *Chem Sus Chem*, 1 (2008) 893.
9 Keith D W, *Science*, 325 (2009) 1654.
10 Wahby A, Ramos-Fernández J M, Martínez-Escandell M, Sepúlveda-Escribano A, Silvestre-Albero J & Rodríguez-Reinoso F, *Chem Sus Chem*, 3 (2010) 974.
11 Freeman S A, Dugas R, Van Wagener D, Nguyen T & Rochelle G T, *Energy Proc*, 1 (2009) 1489.
12 Zhou S, Chen X, Nguyen T, Voice A K & Rochelle G T, *Chem Sus Chem*, 3 (2010) 913.
13 Jensen A & Christensen R, *Acta Chem Scand*, 9 (1955) 486.
14 Trass O & Weiland R H, *Can J Chem Eng*, 49 (1971) 773.
15 Sharma M M, *Trans Faraday Soc*, 61 (1965) 681.
16 Sada E, Kumazawa H & Butt M A, *Chem Eng J*, 13 (1977) 213.
17 Hikita H, Asai S, Ishikawa H & Honda M, *Chem Eng J*, 13 (1977) 7.
18 Li J, Henni A & Tontiwachwuthikul P, *Ind Eng Chem Res*, 46 (2007) 4426.
19 Zhang J, Han B, Zhao Y, Li J, Hou M & Yang G, *Chem Commun*, 47 (2010) 1033.
20 Perry R J, Grocela-Rocha T A, O'Brien M J, Genovese S, Wood B R, Lewis L N, Lam H, Soloveichik G, Rubinsztajn M, Kniajanski S, Draper S, Enick R M, Johnson J K, Xie H-B & Tapriyal D, *Chem Sus Chem*, 3 (2010) 919.
21 Simons K, Nijmeijer K, Mengers H, Brilman W & Wessling M, *Chem Commun*, 3 (2010) 939.
22 Chakravarti S, Gupta A & Hunek B, in *First National Conference on Carbon Sequestration*, Washington DC, 2001.
23 YazaydÄ A O z r, Snurr R Q, Park T-H, Koh K, Liu J, LeVan M D, Benin A I, Jakubczak P, Lanuza M, Galloway D B, Low J J & Willis R R, *J Am Chem Soc*, 131 (2009) 18198.
24 Bae Y-S, Farha O K, Hupp J T & Snurr R Q, *J Mater Chem*, 19 (2009) 2131.
25 YazaydÄ±n A O z r, Benin A I, Faheem S A, Jakubczak P, Low J J, Willis R R & Snurr R Q, *Chem Mat*, 21 (2009) 1425.
26 Bae Y-S, Farha O K, Spokoyny A M, Mirkin C A, Hupp J T & Snurr R Q, *Chem Commun*, (2008) 4135.

27 Siriwardane R V, Shen M-S, Fisher E P & Poston J A, *Energy Fuels*, 15 (2001) 279.
28 Belmabkhout Y & Sayari A, *Chem Eng Sci*, 64 (2009) 3729
29 Himeno S, Komatsu T & Fujita S, *Adsorption*, 11 (2005) 899.
30 Kapoor R & Yang R T, *Chem Eng Sci*, 44 (1989) 1723
31 Freeman B D, *Macromolecules*, 32 (1999) 375.
32 Baker R W, *Indust Eng Chem Res*, 41 (2002) 1393.
33 Goetz V, Pupier O & Guillot A, *Adsorption*, 12 (2006) 55.
34 Alesi W R, Gray M & Kitchin J R, *Chem Sus Chem*, 3 (2010) 948.
35 Eddaoudi M, Kim J, Rosi N, Vodak D, Wachter J, O'Keeffe M & Yaghi O M, *Science*, 295 (2002) 469.
36 Wu H, Simmons J M, Liu Y, Brown C M, Wang X-S, Ma S, Peterson V K, Southon P D, Kepert C J, Zhou H-C, Yildirim T & Zhou W, *Chem – Eur J*, 16 (2010) 5205.
37 Ma S, Sun D, Simmons J M, Collier C D, Yuan D & Zhou H C, *J Am Chem Soc*, 130 (2008) 1012.
38 Lozano-Castell D, AlcaÇiz-Mongea J, de la Casa-Lillo M A, Cazorla-Amor D & Linares-Solano S A, *Fuel*, 81 (2002) 1777
39 Struzhkin V V, Militzer B, Mao W L, Mao H-k & Hemley R J, *Chem Rev*, 107 (2007) 4133.
40 Han S S, Furukawa H, Yaghi O M & Goddard W A, *J Am Chem Soc*, 130 (2008) 11580.
41 Rowsell J L C & Yaghi O M, *Angew Chem Int Ed* , 44 (2005) 4670.
42 Furukawa H & Yaghi O M, *J Am Chem Soc*, 131 (2009) 8875.
43 Schlapbach L & Zuttel A, *Nature*, 414 (2001) 353.
44 Dillon A C, Jones K M, Bekkedahl T A, Kiang C H, Bethune D S & Heben M J, *Nature*, 386 (1997) 377.
45 Liu C, Fan Y Y, Liu M, Cong H T, Cheng H M & Dresselhaus M S, *Science*, 286 (1999) 1127.
46 Ye Y, Ahn C C, Witham C, Fultz B, Liu J, Rinzler A G, Colbert D, Smith K A & Smalley R E, *Appl Phys Lett*, 74 (1999) 2307.
47 Chen Y, Shaw D T, Bai X D, Wang E G, Lund C, Lu W M & Chung D D L, *Appl Phys Lett*, 78 (2001) 2128.
48 Smith M R, Bittner E W, Shi W, Johnson J K & Bockrath B C, *J Phys Chem B*, 107 (2003) 3752.
49 Gundiah G, Govindaraj A, Rajalakshmi N, Dhathathreyan K S & Rao C N R, *J Mater Chem*, 13 (2003) 209.
50 Tibbetts G G, Meisner G P & Olk C H, *Carbon*, 39 (2001) 2291.
51 Rajalakshmi N, Dhathathreyan K S, Govindaraj A & Satishkumar B C, *Electrochim Acta*, 45 (2000) 4511.
52 Guo Z P, Ng S H, Wang J Z, Huang Z G, Liu H K, Too C O & Wallace G G, *J Nanosci Nanotechnol*, 6 (2006) 713.
53 Chen P, Wu X, Lin J & Tan K L, *Science*, 285 (1999) 91.
54 Yang R T, *Carbon*, 38 (2000) 623.
55 Pinkerton F E, Wicke B G, Olk C H, Tibbetts G G, Meisner G P, Meyer M S & Herbst J F, *J Phys ChemB*, 104 (2000) 9460.
56 Reyhani A, Mortazavi S Z, Mirershadi S, Moshfegh A Z, Parvin P & Golikand A N, *J Phys Chem B*, 115 (2011) 6994.
57 Dag S, Ozturk Y, Ciraci S & Yildirim T, *Phys Rev B*, 72 (2005) 155404.
58 Wu H, Wexler D, Ranjbartoreh A R, Liu H & Wang G, *Int J Hydrogen Energy*, 35 (2010) 6345.
59 Miyamoto J, Hattori Y, Noguchi D, Tanaka H, Ohba T, Utsumi S, Kanoh H, Kim Y A, Muramatsu H, Hayashi T, Endo M & Kaneko K, *J Am Chem Soc*, 128 (2006) 12636.
60 Xia Y, Zhu J Z, Zhao M, Li F, Huang B, Ji Y, Liu X, Tan Z, Song C & Yin Y, *Phys Rev B*, 71 (2005) 075412.
61 Ma R, Bando Y, Zhu H, Sato T, Xu C & Wu D, *J Am Chem Soc*, 124 (2002) 7672.
62 Tang C, Bando Y, Ding X, Qi S & Golberg D, *J Am Chem Soc*, 124 (2002) 14550.
63 Terao T, Bando Y, Mitome M, Kurashima K, Zhi C Y, Tang C C & Golberg D, *Physica E*, 40 (2008) 2551.
64 Leela Mohana Reddy A, Tanur A E & Walker G C, *Int J Hydrogen Energy*, 35 (2010) 4138.
65 Wu X, Yang J, Hou J G & Zhu Q, *J Chem Phys*, 121 (2004) 8481.
66 Wu X, Yang J, Hou J G & Zhu Q, *Phys Rev B*, 69 (2004) 153411.
67 Wu X, Yang J, Hou J G & Zhu Q, 124 (2006) 054706.
68 Jhi S-H, *Phys Rev B*, 74 (2006) 155424.
69 Mpourmpakis G & Froudakis G E, *Catal Today*, 120 (2007) 341.
70 Baierle R r J, Piquini P, Schmidt T M & Fazzio A, *J Phys Chem B*, 110 (2006) 21184.
71 Shevlin S A & Guo Z X, *Phys Rev B*, 76 (2007) 024104.
72 Patchkovskii S, Tse J S, Yurchenko S N, Zhechkov L, Heine T & Seifert G, *Proc Natl Acad Sci USA*, 102 (2005) 10439.
73 Ghosh A, Subrahmanyam K S, Krishna K S, Datta S, Govindaraj A, Pati S K & Rao C N R, *J Phys Chem C*, 112 (2008) 15704.
74 Srinivas G, Zhu Y, Piner R, Skipper N, Ellerby M & Ruoff R, *Carbon*, 48 (2010) 630.
75 Jin Z, Lu W, O'Neill K J, Parilla P A, Simpson L J, Kittrell C & Tour J M, *Chem Mat*, 23 (2011) 923.
76 Mpourmpakis G, Tylianakis E & Froudakis G E, *Nano Lett*, 7 (2007) 1893.
77 Li J, Furuta T, Goto H, Ohashi T, Fujiwara Y & Yip S, *J Phys Chem*, 119 (2003) 2376.
78 Pekker S, Salvetat J P, Jakab E, Bonard J M & Forr L, *J Phys Chem B*, 105 (2001) 7938.
79 Nikitin A, Ogasawara H, Mann D, Denecke R, Zhang Z, Dai H, Cho K & Nilsson A, *Phys Rev Lett*, 95 (2005) 225507.
80 Talyzin A V, Luzan S, Anoshkin I V, Nasibulin A G, Jiang H, Kauppinen E I, Mikoushkin V M, Shnitov V V, Marchenko D E & Norel us D, *ACS Nano*, 5 (2011) 5132.
81 Elias D C, Nair R R, Mohiuddin T M G, Morozov S V, Blake P, Halsall M P, Ferrari A C, Boukhvalov D W, Katsnelson M I, Geim A K & Novoselov K S, *Science*, 323 (2009) 610.
82 Jaiswal M, Yi Xuan Lim C H, Bao Q, Toh C T, Loh K P & Oì^zyilmaz B, *ACS Nano*, 5 (2011) 888.
83 Xie L, Jiao L & Dai H, *J Am Chem Soc*, 132 (2010) 14751.
84 Jones J D, Hoffmann W D, Jesseph A V, Morris C J, Verbeck G F & Perez J M, *Appl Phys Lett*, 97 (2010) 233104.
85 Zheng L, Li Z, Bourdo S, Watanabe F, Ryerson C C & Biris A S, *Chem Commun* , 47 (2010) 1213.
86 Subrahmanyam K S, Kumar P, Maitra U, Govindaraj A, Hembram K P S S, Waghmare U V & Rao C N R, *Proc Natl Acad Sci USA*, 108 (2011) 2674.
87 Gopalakrishnan K, Subrahmanyam K S, Kumar P, Govindaraj A & Rao C N R, (doi:10.1039/c1rA00403d.).
88 Stan G, Bojan M J, Curtarolo S, Gatica S M & Cole M W, *Phys Rev B*, 62 (2000) 2173.
89 Williams K A & Eklund P C, *Chem Phys Lett*, 320 (2000) 352.
90 Shi W & Johnson J K, *Phys Rev Lett*, 91 (2003) 015504.

91 LaBrosse M R, Shi W & Johnson J K, *Langmuir,* 24 (2008) 9430.
92 LaBrosse M R & Johnson J K, *J Phys Chem C,* 114 (2010) 7602.
93 Kowalczyk P, Solarz L, Do D D, Samborski A & MacElroy J M D, *Langmuir*, 22 (2006) 9035.
94 Bekyarova E, Murata K, Yudasaka M, Kasuya D, Iijima S, Tanaka H, Kahoh H & Kaneko K, *J Chem Phys B,* 107 (2003) 4681.
95 Murata K, Hashimoto A, Yudasaka M, Kasuya D, Kaneko K & Iijima S, *Adv Mater,* 16 (2004) 1520.
96 Yamamoto M, Itoh T, Sakamoto H, Fujimori T, Urita K, Hattori Y, Ohba T, Kagita H, Kanoh H, Niimura S, Hata K, Takeuchi K, Endo M, RodrÃguez-Reinoso F & Kaneko K, *Adsorption,* 17 (2011) 643.
97 Lee J-W, Kang H-C, Shim W-G, Kim C & Moon H, *J Chem Eng Data,* 51 (2006) 963.
98 Yulong W, Fei W, Guohua L, Guoqing N & Mingde Y, *Mater Res Bull,* 43 (2008) 1431.
99 Albesa A G, Llanos J L & Vicente J L, *Langmuir,* 24 (2008) 3836.
100 Thierfelder C, Witte M, Blankenburg S, Rauls E & Schmidt W G, *Surf Sci,* 605 (2011) 746.
101 Kumar N, Subrahmanyam K S, Chaturbedy P, Raidongia K, Govindaraj A, Hembram K P S S, Mishra A K, Waghmare U V & Rao C N R, *Chem Sus Chem,* 4 (2011) 1662.
102 Janik J F, Ackerman W C, Paine R T, Hua D-W, Maskara A & Smith D M, *Langmuir,* 10 (1994) 514.
103 Zhao J, Buldum A, Han A & Lu J P, *Nanotech,* 13 (2002) 195.
104 Chen L & Johnson J K, *Phys Rev Lett,* 94 (2005) 125701.
105 Kowalczyk P, Furmaniak S, Gauden P A & Terzyk A P, 114 (2010) 21465.
106 Millward A R & Yaghi O M, *J Am Chem Soc,* 127 (2005) 17998.
107 Mackie I D & DiLabio G A, *Phys Chem Chem Phys,* 13 (2011) 2780.
108 Cinke M, Li J, Bauschlicher C W, Ricca A & Meyyappan M, *Chem Phys Lett,* 376 (2003) 761.
109 Hu Y H & Ruckenstein E, *Chem Phys Lett,* 425 (2006) 306.
110 Bienfait M, Zeppenfeld P, Dupont-Pavlovsky N, Muris M, Johnson M R, Wilson T, DePies M & Vilches O E, *Phys Rev B,* 70 (2004) 035410.
111 Mishra A K & Ramaprabhu S, *Energy Environ Sci,* 4 (2010) 889.
112 Su F, Lu C, Cnen W, Bai H & Hwang J F, *Sc Total Environ,* 407 (2009) 3017.
113 Hsu S-C, Lu C, Su F, Zeng W & Chen W, *Chem Eng Sc,* 65 (2010) 1354.
114 Su F, Lu C & Chen H-S, *Langmuir,* 27 (2011) 8090.
115 Dillon E P, Crouse C A & Barron A R, *ACS Nano,* 2 (2008) 156.
116 Matranga C, Chen L, Smith M, Bittner E, Johnson J K & Bockrath B, *J Phys Chem B,* 107 (2003) 12930.
117 Matranga C & Bockrath B, *J Phys Chem B,* 108 (2004) 6170.
118 Cabrera-Sanfelix P, *J Phys Chem A,* 113 (2008) 493.
119 Mishra A K & Ramaprabhu S, *J Mater Chem,* 21 (2011) 7467.
120 Raidongia K, Nag A, Hembram K P S S, Waghmare U V, Datta R & Rao C N R, *Chem–Eur J,* 16 (2010) 149.